J. Fluid Mech. (2014), *vol.* 746, *pp.* 31–52. © Cambridge University Press 2014
doi:10.1017/jfm.2014.117

Speeding up thermocapillary migration of a confined bubble by wall slip

Ying-Chih Liao[1], Yen-Ching Li[3], Yu-Chih Chang[1], Chih-Yung Huang[2] and Hsien-Hung Wei[3],†

[1]Department of Chemical Engineering, National Taiwan University, Taipei 106, Taiwan

[2]Department of Power Mechanical Engineering, National Tsing Hua University, Hsinchu 30013, Taiwan

[3]Department of Chemical Engineering, National Cheng Kung University, Tainan 701, Taiwan

(Received 12 July 2013; revised 9 February 2014; accepted 25 February 2014;
first published online 28 March 2014)

It is usually believed that wall slip contributes small effects to macroscopic flow characteristics. Here we demonstrate that this is not the case for the thermocapillary migration of a long bubble in a slippery tube. We show that a fraction of the wall slip, with the slip length λ much smaller than the tube radius R, can make the bubble migrate much faster than without wall slip. This speedup effect occurs in the strong-slip regime where the film thickness b is smaller than λ when the Marangoni number $S = \tau_T R/\sigma_0$ ($\ll 1$) is below the critical value $S^* \sim (\lambda/R)^{1/2}$, where τ_T is the driving thermal stress and σ_0 is the surface tension. The resulting bubble migration speed is found to be $U_b \sim (\sigma_0/\mu)S^3(\lambda/R)$, which can be more than a hundred times faster than the no-slip result $U_b \sim (\sigma_0/\mu)S^5$ (Wilson, *J. Eng. Math.*, vol. 29, 1995, pp. 205–217; Mazouchi & Homsy, *Phys. Fluids*, vol. 12, 2000, pp. 542–549), with μ being the fluid viscosity. The change from the fifth power law to the cubic one also indicates a transition from the no-slip state to the strong-slip state, albeit the film thickness always scales as $b \sim RS^2$. The formal lubrication analysis and numerical results confirm the above findings. Our results in different slip regimes are shown to be equivalent to those for the Bretherton problem (Liao, Li & Wei, Phys. Rev. Lett., vol. 111, 2013, 136001). Extension to polygonal tubes and connection to experiments are also made. It is found that the slight discrepancy between experiment (Lajeunesse & Homsy, *Phys. Fluids*, vol. 15, 2003, pp. 308–314) and theory (Mazouchi & Homsy, *Phys. Fluids*, vol. 13, 2001, pp. 1594–1600) can be interpreted by including wall slip effects.

Key words: interfacial flows (free surface), lubrication theory, thin films

1. Introduction

When a bubble is subjected to a temperature gradient, it can migrate due to thermocapillary effects. Specifically, because the surface tension is lower (higher) at the hot (cold) end, the resulting surface tension gradient can drive the surrounding liquid towards the cold end, and the viscous opposition on the liquid side in turn makes the bubble move towards the hot end (Young, Goldstein & Block 1959). A similar effect can be used to drive liquid droplets on substrates along applied

† Email address for correspondence: hhwei@mail.ncku.edu.tw

Downloaded from https://www.cambridge.org/core. National Cheng Kung University, on 21 Jul 2020 at 05:08:35, subject to the Cambridge Core terms of use, available at https://www.cambridge.org/core/terms. https://doi.org/10.1017/jfm.2014.117

temperature gradients (Brzoska, Brochard-Wyart & Rondelez 1993; Smith 1995; Pratap, Moumen & Subramanian 2008; Gomba & Homsy 2010; Nguyen & Chen 2010; Karapetsas, Sahu & Matar 2013). Such thermocapillary actuation also has potential applications in microfluidics (Darhuber *et al.* 2003; Baroud *et al.* 2007; Selva *et al.* 2010), because it not only provides an efficient means to drive fluids in small scales but also enables flows to be manipulated without moving parts.

Here we are more interested in the thermocapillary motion of fluid particles in *confined* geometries, as occurring in enhanced oil recovery and microfluidic devices. In enhanced oil recovery, water is injected into hot porous rocks underground to facilitate extraction of residual oil (Slattery 1974). Much like viscous fingering in porous media (Saffman & Taylor 1958; Homsy 1987), a water slug can form in a small capillary pore to displace more viscous oil, entraining oil to create a thin film beneath the slug. The problem is closely related to the classical Bretherton problem, in which a long bubble travels at a constant velocity in a closed tube (Bretherton 1961). But there is one important difference: the additional thermocapillary stress on the bubble surface can render extra fluid entrainment into the film towards the cold end, which can help the water slug gain more speed moving into the pore. A similar situation can also occur in thermally actuated microfluidic devices, where fluid particles can be transported under the action of thermocapillary forces (Jiao *et al.* 2008; Selva *et al.* 2010).

There are a number of studies addressing how confined boundaries affect the thermocapillary motion of fluid particles. Wilson (1993) first analysed the thermocapillary-driven motion of a large droplet in a closed tube subject to a constant axial temperature gradient. In his later work, he showed, using lubrication analysis, that the film thickness can grow quadratically with the Marangoni number M (i.e. S in the present work), where M measures the strength of the applied thermocapillary stress over the droplet surface. More importantly, he found that the droplet can migrate at a speed proportional to M^5 (Wilson 1995). The same results were rediscovered, also using lubrication analysis, by Mazouchi & Homsy (2000), who studied the same problem with a long bubble. Such a strong dependence of the droplet/bubble speed on the driving thermal stress is actually a combined consequence of thermocapillary film entrainment (in terms of $(b/R)^{3/2}$ according to Bretherton's law) and its conversion (of a factor b/R, the ratio of the film thickness to the tube radius) into the droplet/bubble displacement in the opposite direction due to fluid mass conservation (Mazouchi & Homsy 2000; Stone 2010). It is worth noting that the shape of the tube cross-section could have a strong impact on a problem of this sort. In an analysis extended to a polygonal tube by Mazouchi & Homsy (2001), they found that a bubble actually travels at a speed linearly proportional to the applied temperature gradient due to the much greater thermocapillary flow through the corner regions of the tube.

In this work we extend previous studies by Wilson (1995) and Mazouchi & Homsy (2000) to look at how wall slip influences the thermocapillary motion of a long bubble in a cylindrical tube. In contrast to existing studies that assume the no-slip condition, the problem here is relevant to a more realistic situation where considerable wall slip can exist due to nanobubbles or gas pockets trapped on solid surfaces (Tyrrell & Attard 2001), or due to chemical treatments or surface structures (Craig, Neto & Williams 2001; Choi & Kim 2006). Because wall slip can reduce viscous drag, we anticipate that a bubble should move faster than in the no-slip case. This immediately raises two questions: (i) How much faster can the bubble move? (ii) How does the bubble velocity depend on the applied temperature gradient and the tube size? In this paper, we will address these questions by extending the previous no-slip analyses

Downloaded from https://www.cambridge.org/core. National Cheng Kung University, on 21 Jul 2020 at 05:08:35, subject to the Cambridge Core terms of use, available at https://www.cambridge.org/core/terms. https://doi.org/10.1017/jfm.2014.117

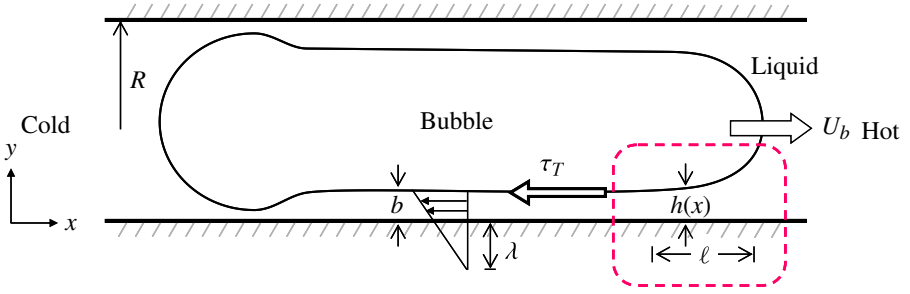

FIGURE 1. Schematic diagram for the thermocapillary motion of a long bubble in a capillary tube. A temperature gradient produces an interfacial stress τ_T to pull the fluid towards the cold end, making the bubble move towards the hot end. Here we look at the film flow in the transition zone of size $\ell \sim (bR)^{1/2}$, as indicated by the box.

mentioned above to see how the bubble speed varies with the extent of wall slip. Below we briefly explain how the problem is motivated from a fundamental point of view and why we expect to see new physics for this problem due to the breakdown of the no-slip condition.

The effects of wall slip are often described by the Navier slip condition at a slippery surface $(y = 0)$,

$$u = \lambda \frac{\partial u}{\partial y}, \tag{1.1}$$

where the amount of slip is measured by the slip length λ, defined as the ratio of the slip velocity $u(y = 0)$ to the corresponding shear rate $\partial u/\partial y$ (Navier 1823). Because λ typically ranges between 100 nm and 1 μm (Lauga, Brenner & Stone 2007), and most interfacial flows have much greater depths of the order of 100 μm, one might think that wall slip merely contributes small effects. However, this might be overshadowed by the fact that the liquid thickness b, especially in ultrathin film flows, can sometimes be comparable to or smaller than λ, so that slip effects can become strong enough to alter the flow characteristics qualitatively. To better elucidate this point, let us consider the present problem, where a long bubble is moving in a slippery capillary tube (of radius $R \gg \lambda$) (see figure 1), and imagine what happens when the driving thermocapillary stress τ_T on the bubble surface is varied.

At large τ_T, because of strong fluid entrainment into the film, the film can be so thick that $b \gg \lambda$. Much like the no-slip case, the film thickness in this case should vary quadratically with τ_T (Wilson 1995; Mazouchi & Homsy 2000). As the film gets thinner by lowering τ_T, the importance of wall slip grows progressively. When the film thickness is down to the point where $b \sim \lambda$, the departure from the no-slip condition starts to become more apparent. Further lowering τ_T decreases b below λ, and can lead the flow to be much amplified by slip effects. In fact, the Navier slip condition (1.1) immediately implies that, when $\lambda > b$, the velocity scale in the film can be amplified by a factor λ/b. So in this strong-slip regime, because λ must enter to characterise the problem, we anticipate that the usual scaling laws based on the no-slip condition will no longer be valid. New scaling laws must emerge to govern how both the film thickness and the bubble speed vary with τ_T. This also implies that, when decreasing τ_T from large to small values, there must exist a *no-slip to slip transition* accompanied by such scaling law changes. In our recent study on the Bretherton problem with wall slip, we show that the well-known 2/3 law can turn into a new

Downloaded from https://www.cambridge.org/core. National Cheng Kung University, on 21 Jul 2020 at 05:08:35, subject to the Cambridge Core terms of use, available at https://www.cambridge.org/core/terms.
https://doi.org/10.1017/jfm.2014.117

quadratic law when slip effects become important (Li *et al.* 2014). In fact, we have recently demonstrated that slip effects can substantially modify the hydrodynamics for a wide range of *free-surface* film flows (Liao, Li & Wei 2013), as also revealed by a number of previous studies (Sharma & Kargupta 2003; Kargupta, Sharma & Khanna 2004; Hu 2005; Münch 2005; Münch & Wagner 2005; Münch, Wagner & Witelski 2005). Here we will show that a similar flow characteristic change can also occur to the *stress-driven* flows considered in the present study.

The paper is organised as follows. In § 2 we develop a scaling theory to identify how the film thickness b and the bubble speed U_b are influenced by slip effects. To test the theory, we will also carry out a formal lubrication analysis in § 3 to derive the equations for determining b and U_b numerically. Calculated results are presented in § 4, confirming the scaling results found in § 2. Extension to polygonal tubes and connection to experiments will also be made in § 5. The paper is concluded in § 6.

2. Scaling analysis

Our goal here is to determine the unknown film thickness b and the bubble speed U_b. Specifically, we seek how they vary with the following variables: the applied thermocapillary stress τ_T, the tube radius R, the slip length λ, the bubble length L_b, the liquid viscosity μ, and the surface tension σ_0. From a purely dimensional standpoint, we can scale b and U_b respectively by R and σ_0/μ, and express them in terms of *dimensionless* variables $\tau_T R/\sigma_0$, λ/R and L_b/R. We further assume that the relationships take the power-law forms

$$\frac{b}{R} = k_1 \left(\frac{\tau_T R}{\sigma_0}\right)^{\alpha_1} \left(\frac{\lambda}{R}\right)^{\beta_1} \left(\frac{L_b}{R}\right)^{\gamma_1}, \tag{2.1a}$$

$$\frac{U_b}{\sigma_0/\mu} = k_2 \left(\frac{\tau_T R}{\sigma_0}\right)^{\alpha_2} \left(\frac{\lambda}{R}\right)^{\beta_2} \left(\frac{L_b}{R}\right)^{\gamma_2}, \tag{2.1b}$$

with k_1 and k_2 being numerical prefactors. Here we are more concerned with the values of the exponents α_i, β_i and γ_i $(i = 1, 2)$, which will be determined by how the relevant effects are balanced according to physical laws. According to Wilson (1995) and Mazouchi & Homsy (2000) for the no-slip case, the values of these exponents are $\alpha_1 = 2$, $\alpha_2 = 5$, $\beta_1 = \beta_2 = 0$ and $\gamma_1 = \gamma_2 = 0$. But if λ is non-zero, especially when slip effects are strong at low τ_T, we expect that the scaling relationships (2.1*a*) and (2.1*b*) would differ from those in the no-slip case. As we shall demonstrate below, the results actually depend strongly on the extent of wall slip, distinguished by three distinct regimes: *weak slip*, *strong slip* and *super slip*.

2.1. *Weak-slip regime*

In the weak-slip regime, where $b \gg \lambda$ at sufficiently high τ_T, the situation is dictated by the usual no-slip scenario. Though this case has been studied previously (Wilson 1995; Mazouchi & Homsy 2000), it is worth while to review how to derive the scaling laws physically. This will not only allow us to understand how relevant effects are at play, but also provide us with hints about how the scaling laws are modified by wall slip in the later analysis. Similar to the classical Bretherton problem (Bretherton 1961), all the relevant effects occur in the transition zone (of $\ell \sim (bR)^{1/2}$ in length) between the uniform film (of thickness b) and the meniscus region (of radius $\sim R$). Figure 2(*a*) sketches the basic flow mechanism. Because of the imposed temperature gradient over the film, $G_b \equiv |\partial T_b/\partial x|$ (across the bubble length L_b), the liquid can

Downloaded from https://www.cambridge.org/core. National Cheng Kung University, on 21 Jul 2020 at 05:08:35, subject to the Cambridge Core terms of use, available at https://www.cambridge.org/core/terms.
https://doi.org/10.1017/jfm.2014.117

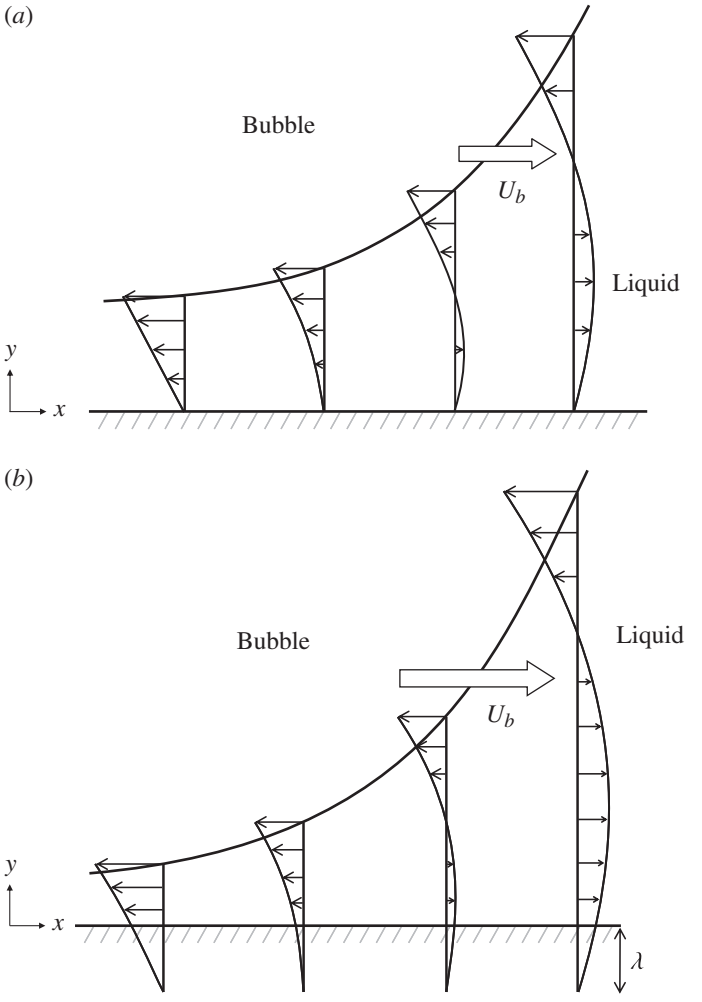

FIGURE 2. Thermocapillary liquid entrainment in the transition film region on (*a*) a no-slip wall and (*b*) a slippery wall. While the thermocapillary stress tends to drive the fluid *into* the film, the capillary pressure gradient tends to drain the fluid *out of* the film. The flow rate imbalance between these two mechanisms sets the bubble in motion as a consequence of no net flow rate across the tube diameter. When wall slip is present, both thermocapillary and capillary flows are enhanced. But capillary draining becomes much more intensified in the thicker part of the film, making the film thinner compared to the no-slip case. Also because of this slip-enhanced capillary draining, the bubble will move faster.

be entrained into the film under the action of the thermocapillary stress $\tau_T = G_b\beta$, where $\beta = -\partial\sigma/\partial T$ (>0) measures the susceptibility to lowering the surface tension σ by raising the temperature T. By balancing τ_T to the viscous stress $\mu u_T/b$, this flow entrainment has a velocity scale given by

$$u_T \sim \tau_T b/\mu. \tag{2.2}$$

On the other hand, this flow has to distort the round bubble meniscus that remains almost hydrostatic everywhere except the portion near the wall (provided that the

Downloaded from https://www.cambridge.org/core. National Cheng Kung University, on 21 Jul 2020 at 05:08:35, subject to the Cambridge Core terms of use, available at https://www.cambridge.org/core/terms.
https://doi.org/10.1017/jfm.2014.117

surface tension here is sufficiently strong). Because the thicker part of the film has a greater interfacial curvature, this generates a more negative capillary pressure $p \sim \sigma_0 b/\ell^2 \sim \sigma_0/R$ to suck the fluid out of the film. The velocity scale u_{cap} for this capillary draining can be estimated by balancing the viscous force (per unit depth) $\mu u_{cap}/b^2$ to the capillary pressure gradient $p/\ell \sim (\sigma_0/R^2)(b/R)^{-1/2}$, giving

$$u_{cap} \sim (b/R)^{3/2}(\sigma_0/\mu). \tag{2.3}$$

The film thickness can then be estimated by equating (2.2) to (2.3):

$$\frac{b}{R} \sim \left(\frac{\tau_T R}{\sigma_0}\right)^2. \tag{2.4}$$

The same result can be obtained by using Bretherton's 2/3 law, $b/R \sim Ca_f^{2/3}$, with the capillary number $Ca_f = \mu u_T/\sigma_0 = (\tau_T R/\sigma_0)(b/R)$ based on the driving film velocity u_T given by (2.2) (Stone 2010). Because the entrainment flow rate $2\pi u_T bR$ across the film must be equal to the displacement flow rate $\pi U_b R^2$ across the tube, the resulting bubble migration speed is then $U_b \sim u_T(b/R) \sim (\tau_T R/\mu)(b/R)^2$. Together with (2.4), this becomes

$$U_b \sim \left(\frac{\tau_T R}{\sigma_0}\right)^5 \frac{\sigma_0}{\mu}. \tag{2.5}$$

Both (2.4) and (2.5) were first reported by Wilson (1995) and later rediscovered by Mazouchi & Homsy (2000). These results have also been rederived by Stone (2010) using the same scaling arguments as above.

It is worth pointing out that, while the driving stress here, $\tau_T = G_b\beta$, is given by the temperature gradient $G_b \equiv |\partial T_b/\partial x|$ over the film across the bubble length L_b, it is often sustained by the prescribed *global* temperature gradient $G \equiv |\partial T/\partial x|$ across the tube length L. Because the total heat flow across the film must be equal to that across the tube's diameter, if $L \gg L_b$ we can write $2\pi RbG_b \approx G\pi R^2$, so the temperature gradient over the film G_b is actually steepened by a factor $R/2b$ compared to the global one G (provided that the heat transfer is dominated by heat conduction and the thermal conductivity of the bubble is negligible). Hence, written in terms of G, τ_T is also amplified by the same factor $R/2b$:

$$\tau_T \approx (R/2b)G\beta. \tag{2.6}$$

Because of this, $u_T \sim \tau_T b/\mu$ in (2.2) reduces to $G\beta R/\mu$, which is independent of b. Then (2.4) and (2.5) can be rewritten as

$$\frac{b}{R} \sim \left(\frac{G\beta R}{\sigma_0}\right)^{2/3}, \tag{2.7}$$

$$U_b \sim \left(\frac{G\beta R}{\sigma_0}\right)^{5/3} \frac{\sigma_0}{\mu}. \tag{2.8}$$

Here $G\beta R/\sigma_0$ is exactly the film capillary number $Ca_f = \mu u_T/\sigma_0$ mentioned earlier. As a result, the film thickness follows Bretherton's 2/3 law (2.7), leading the bubble speed to obey the 5/3 law (2.8). Unlike the *unbounded* case, in which $U_b \sim (G\beta R/\sigma_0)(\sigma_0/\mu)$ (wherein R is the bubble radius) (Young *et al.* 1959; Subramanian 1981), U_b given by (2.8) is *not* linear in G but is proportional to $G^{5/3}$ because of the factor R/b temperature steepening by the film. Alternatively, since the bubble motion here is dissipated by much greater viscous forces over the film, the resulting bubble speed (2.8) is slower by a factor of $b/R \sim (G\beta R/\sigma_0)^{2/3}$ than in the unbounded case.

Downloaded from https://www.cambridge.org/core. National Cheng Kung University, on 21 Jul 2020 at 05:08:35, subject to the Cambridge Core terms of use, available at https://www.cambridge.org/core/terms.
https://doi.org/10.1017/jfm.2014.117

2.2. *Strong-slip regime*

Now we discuss the effects of wall slip. Figure 2(*b*) shows how wall slip modifies the picture compared to figure 2(*a*) without slip. How slip effects kick in can be pictured by gradually lowering τ_T from the weak-slip regime. According to (2.4), the lower τ_T, the thinner b. So if τ_T is lowered to the point where b is comparable to or below λ, we enter the strong-slip regime in which all the no-slip results shown above will cease to hold. The critical stress τ_T^* for this to happen can be estimated using (2.4) with $b \sim \lambda$:

$$\frac{\tau_T^* R}{\sigma_0} \sim \left(\frac{\lambda}{R}\right)^{1/2}. \tag{2.9}$$

In this strong-slip regime, the thermocapillary velocity (2.2) is amplified to

$$u_T' \sim (\lambda/b) u_T \sim \lambda \tau_T/\mu. \tag{2.10}$$

The capillary velocity (2.3) is also amplified to the same extent: $u_{cap}' \sim (\lambda/b) u_{cap}$. So balancing these two velocity scales $u_T' \sim u_{cap}'$ gives exactly the same scaling (2.4) for b as in the no-slip case. Note that this does not imply that the film thickness here is the same as in the no-slip case, since the former has to be thinner than the latter, as physically required here. This will also be confirmed later in § 4. But in terms of the bubble speed, it does have a different scaling as shown below.

Using $U_b \sim u_T' b/R$ together with (2.10) and (2.4), the bubble speed scales as

$$U_b \sim \left(\frac{\tau_T R}{\sigma_0}\right)^3 \left(\frac{\lambda}{R}\right) \frac{\sigma_0}{\mu}. \tag{2.11}$$

If a connection is made between the film thickness b/R and the film capillary number $u_T'\mu/\sigma_0$ (via writing $U_b \sim u_T' b/R$ on the left-hand side and replacing $\tau_T R/\sigma_0$ by $(b/R)^{1/2}$ using (2.4) on the right-hand side of (2.11)), we find that (2.11) can be rewritten as

$$\frac{b}{R} \sim \left(\frac{\mu u_T'}{\sigma_0}\right)^2 \left(\frac{R}{\lambda}\right)^2, \tag{2.12}$$

which is essentially the new quadratic law for the Bretherton problem under the strong-slip condition (Liao *et al.* 2013; Li *et al.* 2014).

Compared to the no-slip result (2.5), the bubble speed given by (2.11) is faster by a factor $(\lambda/R)(\tau_T R/\sigma_0)^{-2} > 1$ (because τ_T here is below the critical value (2.9)). Also, $U_b \propto R^2$ has a weaker dependence on R, but can increase linearly with λ. Written in terms of the global temperature gradient G, because $\tau_T \sim (R/b) G\beta \sim (G\beta R/\sigma_0)^{1/3}(\sigma_0/R)$ from (2.6) and (2.7), (2.11) can be re-expressed as

$$U_b \sim \left(\frac{G\beta\lambda}{\sigma_0}\right) \frac{\sigma_0}{\mu}. \tag{2.13}$$

In this way, the bubble speed grows linearly with G, but now is independent of R. Interestingly, (2.13) takes a form quite similar to $(G\beta R/\sigma_0)(\sigma_0/\mu)$ found for the unbounded case (Young *et al.* 1959) – they vary linearly with G. But compared to the unbounded case, (2.13) for the confined case is of $O(\lambda/R)$ slower. This $O(\lambda/R)$ velocity reduction can be attributed to the fact that, even in this strong-slip limit, the bubble motion is still dissipated viscously by the film, with the dissipation not over the film thickness but over the much greater slip length.

Downloaded from https://www.cambridge.org/core. National Cheng Kung University, on 21 Jul 2020 at 05:08:35, subject to the Cambridge Core terms of use, available at https://www.cambridge.org/core/terms. https://doi.org/10.1017/jfm.2014.117

2.3. *Super-slip regime*

In the above analysis, even in the strong-slip situation with $\lambda > b$, we have assumed that the film velocity gradient in y is much greater than that in x, i.e. $\partial u/\partial y \gg \partial u/\partial x$, so that the lubrication approximation can still hold. But if the film happens to be ultrathin at very small τ_T such that the slip length λ is much greater than the lateral length scale $\ell \sim (bR)^{1/2}$ (while still kept $\ll R$), the flow in the film would look like a *plug flow*. Much like the spreading of a droplet on a much less viscous liquid (Brochard-Wyart, Debrégeas & de Gennes 1996), the film flow here will be dissipated more on the lateral side of the film, $\mu\,\partial u/\partial x \sim \mu u/\ell$, than on the vertical side, $\mu\,\partial u/\partial y \sim \mu u/\lambda$. So in this *super*-slip regime, the driving stress τ_T has to be balanced by the lateral viscous stress $\mu u_T'/\ell$, giving the thermocapillary velocity scale $u_T' \sim \tau_T \ell/\mu$ in the film. Note that the film velocity scale here, because viscous dissipation now takes place over the much *larger* length scale ℓ, appears much *lower* than the $\tau_T \lambda/\mu$ given by (2.10) for the strong-slip case. Because of this, the resulting bubble speed in this regime will also be slower than in the strong-slip case, as will be shown later.

Similarly, the velocity scale u_{cap}' for capillary draining can be found by balancing the Laplace pressure gradient $\partial p/\partial x \sim \sigma_0 b/\ell^3$ to the viscous stress gradient $\mu\,\partial^2 u/\partial x^2 \sim \mu u_{cap}'/\ell^2$ on the lateral side, giving $u_{cap}' \sim (\sigma_0/\mu)(b/\ell)$ (Liao *et al.* 2013). Making $u_T' \sim u_{cap}'$, we find $\tau_T \sim \sigma_0 b/\ell^2 \sim \sigma_0/R$ scaling like the Laplace pressure. Therefore, the velocity in the film scales as

$$u_T' \sim \tau_T \ell/\mu \sim (\sigma_0/\mu)(b/R)^{1/2}. \tag{2.14}$$

By making a connection to the film capillary number $\mu u_T'/\sigma_0$, the above relationship can also be written in the alternative form

$$\frac{b}{R} \sim \left(\frac{\mu u_T'}{\sigma_0}\right)^2, \tag{2.15}$$

which is actually the super-slip scaling for the Bretherton problem found by Liao *et al.* (2013).

Now suppose that the bubble is moving in a much longer tube so that its motion is driven by the much intensified driving stress $\tau_T \sim (R/b)G\beta$ (see (2.6)). Balancing it to $\tau_T \sim \sigma_0/R$ found earlier, the film thickness has a scale of

$$\frac{b}{R} \sim \frac{G\beta R}{\sigma_0}. \tag{2.16}$$

Making use of $U_b \sim u_T'(b/R)$ and (2.14), the bubble speed is found to be

$$U_b \sim \left(\frac{G\beta R}{\sigma_0}\right)^{3/2} \frac{\sigma_0}{\mu}. \tag{2.17}$$

Compared to (2.7) and (2.13) for the strong-slip case, the film thickness is thinner by a factor $(G\beta R/\sigma_0)^{1/3}$ (recall that b for the strong-slip case has the same scaling as in the no-slip case). The bubble, however, does not gain more speed because of the super-slipping wall. Instead, it is slower by a factor $(G\beta R/\sigma_0)^{1/2}(R/\lambda) \ll 1$ (owing to the fact that $G\beta R/\sigma_0 \ll (\lambda/R)^2 \ll 1$, derived from the super-slip condition $\lambda \gg \ell$ and (2.16)), as it comes from the much slower film velocity scale (2.14) compared

Downloaded from https://www.cambridge.org/core. National Cheng Kung University, on 21 Jul 2020 at 05:08:35, subject to the Cambridge Core terms of use, available at https://www.cambridge.org/core/terms. https://doi.org/10.1017/jfm.2014.117

	No slip $b \gg \lambda$		Strong slip $b \ll \lambda \ll \ell$		Super slip $b \ll \ell \ll \lambda$ and $\lambda \ll R$
$B = b/R$	S^2	$M^{2/3}$	S^2	$M^{2/3}$	M
$Ca_b = U_b\mu/\sigma_0$	S^5	$M^{5/3}$	$(\lambda/R)S^3$	$(\lambda/R)M$	$M^{3/2}$
$Ca_f = u_T'\mu/\sigma_0$	$B^{3/2}$		$B^{1/2}(\lambda/R)$		$B^{1/2}$

TABLE 1. Summary of the various film thickness b and bubble speed U_b scalings found in the three different regimes of (i) weak slip, (ii) strong slip and (iii) super slip, depending on the size of the slip length λ relative to the film thickness b and to the lateral length scale of the film $\ell \sim (bR)^{1/2}$. In dimensionless form, this shows how $B = b/R$ and the bubble capillary number $Ca_b = U_b\mu/\sigma_0$ vary with different powers of $S = R\tau_T/\sigma_0$ (which measures the strength of the thermocapillary stress τ_T), or of $M = G\beta R/\sigma_0$ (which measures the strength of the global temperature gradient G) if the bubble is moving in a much longer tube. The last row highlights that these findings can be made exactly like the results for the Bretherton problem (Liao *et al.* 2013) if they are re-expressed in terms of the film capillary number $Ca_f = u_T'\mu/\sigma_0$ and the dimensionless film thickness B.

to (2.10) in the strong-slip case. Nevertheless, compared to (2.8) for the no-slip case, (2.17) is indeed faster (by a factor of $(G\beta R/\sigma_0)^{-1/6}$).

For even larger slip length, such as $\lambda \gg R$, there will be virtually no velocity gradient at all in the film to generate viscous drag to slow down the bubble. In other words, the wall of the tube will not have any influence on the bubble. So the bubble in this case will move at speed $U_b \sim (G\beta R/\sigma_0)(\sigma_0/\mu)$ as if it were in an unbounded fluid (Young *et al.* 1959).

2.4. *Summary of different scaling results and their connections*

Table 1 summarises the various scaling results found above. These results are also found to be equivalent to those for the Bretherton problem (Liao *et al.* 2013).

To get a better overall picture of how the results change from one regime to another, below we summarise our findings and make connections in terms of how the bubble speed U_b (reflected by the bubble capillary number $Ca_b = \mu U_b/\sigma_0$) varies with the applied global temperature gradient G (reflected by the Marangoni number $M = G\beta R/\sigma_0$) as sketched in figure 3.

At a sufficiently high G, because $b \gg \lambda$, U_b follows the usual no-slip scaling (2.8) $Ca_b \sim M^{5/3}$, with the film thickness obeying Bretherton's law $b \sim RM^{2/3}$ from (2.7). But (2.8) will only hold up to the point where $b \sim \lambda$ at $M_1^* \sim (\lambda/R)^{3/2}$ (which is obtained by setting $b \sim \lambda$ in the 2/3 law above and essentially (2.9) if writing $M = G\beta R/\sigma_0$ back into $S = \tau_T R/\sigma_0$ using (2.6)). Below this no-slip breakdown point, we enter the strong-slip regime where $b \ll \lambda$ at low G such as $M \ll M_1^*$. In this regime, U_b follows the linear law (2.13): $Ca_b \sim M(\lambda/R)$ faster than in the no-slip case $Ca_b \sim M^{5/3}$, and b still obeys the same scaling (2.7) as in the no-slip case.

At even lower G such that the film becomes ultrathin, like $b \ll \lambda^2/R$, when the film's lateral length scale $\ell \ll \lambda$ turns the film flow into a plug flow, we enter the super-slip regime. The bubble in this regime can travel according to (2.17): $Ca_b \sim M^{3/2}$. It still moves faster than in the no-slip case, $Ca_b \sim M^{5/3}$, but at a speed *slower* than in the strong-slip case, $Ca_b \sim M(\lambda/R)$. The film thickness here scales as $b \sim RM$ from (2.16) and hence is thinner than the $b \sim RM^{2/3}$ found for both the no-slip and strong-slip cases. This regime starts at around the value of G corresponding to

Downloaded from https://www.cambridge.org/core. National Cheng Kung University, on 21 Jul 2020 at 05:08:35, subject to the Cambridge Core terms of use, available at https://www.cambridge.org/core/terms. https://doi.org/10.1017/jfm.2014.117

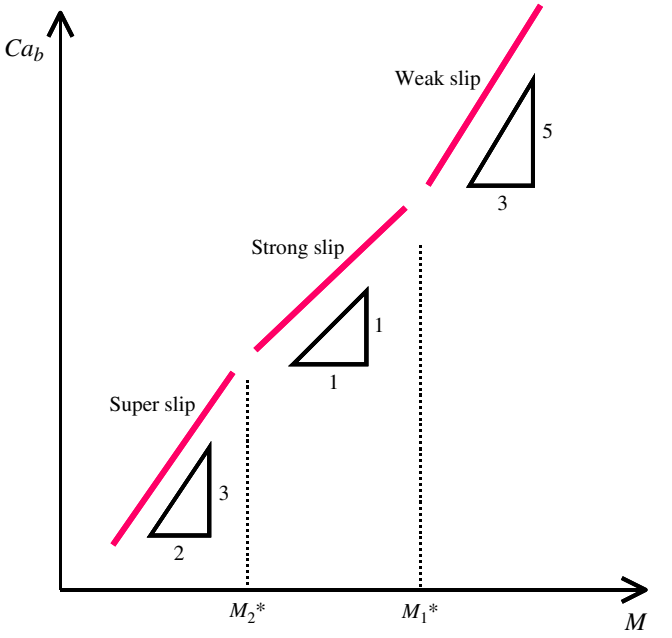

FIGURE 3. Schematic sketch of how the bubble capillary number $Ca_b = \mu U_b/\sigma_0$ varies with the Marangoni number $M = G\beta R/\sigma_0$ (in a log–log scale) in weak-slip, strong-slip and super-slip regimes. As slip effects gradually become strong by lowering M from large to small values, the bubble speed U_b first follows $Ca_b \sim M^{5/3}$ (weak slip) for $M > M_1^*$, then $Ca_b \sim (\lambda/R)M$ (strong slip) for $M_2^* < M < M_1^*$, and finally $Ca_b \sim M^{3/2}$ (super slip) for $M < M_2^*$, where $M_1^* \sim (\lambda/R)^{3/2}$ and $M_2^* \sim (\lambda/R)^2$ mark the transition points in between these regimes.

$M_2^* \sim (\lambda/R)^2$, the crossover between the strong-slip scaling $Ca_b \sim M(\lambda/R)$ and the super-slip scaling $Ca_b \sim M^{3/2}$.

In short, as slip effects gradually become strong by lowering M from large to small values, the bubble speed U_b first follows $Ca_b \sim M^{5/3}$ (weak slip) for $M > M_1^*$, then $Ca_b \sim (\lambda/R)M$ (strong slip) for $M_2^* < M < M_1^*$, and finally turns to $Ca_b \sim M^{3/2}$ (super slip) for $M < M_2^*$, where $M_1^* \sim (\lambda/R)^{3/2}$ and $M_2^* \sim (\lambda/R)^2$ mark the transition points in between these regimes.

Finally, we should emphasise that the above findings are closely connected to the results for the Bretherton problem (Liao *et al.* 2013). If rewritten in terms of $B = b/R$ and the film capillary number $Ca_f = \mu u_T'/\sigma_0$ by noting that $Ca_f = Ca_b/B$ due to $U_b \sim Bu_T'$, all the results – namely, $Ca_b \sim M^{5/3}$ (with $B \sim M^{2/3}$) for weak slip, $Ca_b \sim M(\lambda/R)$ (with $B \sim M^{2/3}$) for strong slip, and $Ca_b \sim M^{3/2}$ (with $B \sim M$) for super slip – turn out to become exactly like those for the Bretherton problem (Liao *et al.* 2013): $Ca_f \sim B^{3/2}$, $Ca_f \sim B^{1/2}(\lambda/R)$ and $Ca_f \sim B^{1/2}$, respectively, which are also summarised in table 1.

3. Lubrication analysis

In this section we extend the lubrication analysis by Mazouchi & Homsy (2000) to derive the relevant equations for determining b and U_b numerically. In addition to confirming their no-slip results, we would mainly like to test the strong-slip scalings

Downloaded from https://www.cambridge.org/core. National Cheng Kung University, on 21 Jul 2020 at 05:08:35, subject to the Cambridge Core terms of use, available at https://www.cambridge.org/core/terms. https://doi.org/10.1017/jfm.2014.117

(2.4) and (2.11) that we find in the preceding section (the super-slip scalings (2.16) and (2.17) will be tested in future work since the usual lubrication theory is not applicable to this case). In a fixed frame, we first solve $\mu\,\partial^2 u/\partial y^2 = \partial p/\partial x$ (along the bubble's moving direction x) to determine the velocity profile in the transition zone,

$$u = \frac{1}{2\mu}\frac{\partial p}{\partial x}(y^2 - 2h(y+\lambda)) + \frac{1}{\mu}\frac{\partial \sigma}{\partial x}(y+\lambda), \tag{3.1}$$

which satisfies the slip condition (1.1) at the wall $y=0$ and $\mu\,\partial u/\partial y = \partial\sigma/\partial x \equiv -\tau_T$ at the air–liquid interface $y=h$. The pressure p can be approximated as the axial Laplace pressure across the interface:

$$p = -\sigma_0 \frac{\partial^2 h}{\partial x^2}. \tag{3.2}$$

The flow rate (per unit width) across the film is then

$$q = \frac{1}{3\mu}\left(-\frac{\partial p}{\partial x}\right)(h^3 + 3\lambda h^2) - \frac{\tau_T}{2\mu}(h^2 + 2\lambda h). \tag{3.3}$$

Taking a mass balance over the zone, at steady state q has to be equal to the net flow rate $q_{net} = U_b(h-b) - (\tau_T/\mu)(b^2/2 + \lambda b)$ coming from the bubble's sweeping and the thermocapillary flow (in the opposite direction) towards the uniform film region. Note that, in the film flow part, we have taken into account the contribution $(\tau_T/\mu)\lambda b$ from the slippery wall. Substituting (3.2) into $q = q_{net}$, we can obtain a differential equation describing how the interface varies with position. Non-dimensionalised by $H = h/R$, $X = x/R$, $\Lambda = \lambda/R$ and $B = b/R$, the equation takes the form

$$\tfrac{1}{3}H_{XXX}(H^3 + 3\Lambda H^2) - \tfrac{1}{2}S(H-B)(H+B+2\Lambda) = Ca_b(H-B). \tag{3.4}$$

Here $S = \tau_T R/\sigma_0$ is the Marangoni number in terms of the thermocapillary velocity $\tau_T R/\mu$ over the bubble scale. In connection with the global temperature gradient $G = 2\tau_T B\beta^{-1}$ (see (2.6)), S should read as $S = \frac{1}{2}(G\beta R/\sigma_0)/B$. Here $Ca_b = \mu U_b/\sigma_0$ is the capillary number based on the (unknown) bubble speed U_b.

Note that in (3.4) both Ca_b and B need to be determined in order to find the unknowns U_b and b. As in Mazouchi & Homsy (2000), the relationship between U_b and b can be established by the global mass balance, in that the flow injection into the uniform film region, $(\tau_T/\mu)(b^2/2 + \lambda b)2\pi R$, is equal to the flow rate generated by the bubble displacement, $\pi U_b R^2$. In terms of the dimensionless form, this global mass balance reads

$$Ca_b = S(B^2 + 2\Lambda B), \tag{3.5}$$

providing a coupling between the unknowns Ca_b and B when coming to solve (3.4). Similar to previous studies (Bretherton 1961; Mazouchi & Homsy 2000), to solve the problem the following boundary conditions are required:

$$H \to B, \quad H_X \to 0, \quad H_{XX} \to 0 \quad \text{as } X \to -\infty, \tag{3.6a}$$

$$H_{XX} \to 1 \quad (\text{or } H \to X^2/2) \quad \text{as } X \to \infty. \tag{3.6b}$$

Prior to taking (3.4)–(3.6) for solving the problem, it is instructive to inspect whether they reveal the features in both the no-slip and strong-slip limits shown

Downloaded from https://www.cambridge.org/core. National Cheng Kung University, on 21 Jul 2020 at 05:08:35, subject to the Cambridge Core terms of use, available at https://www.cambridge.org/core/terms. https://doi.org/10.1017/jfm.2014.117

in § 2. In the no-slip limit ($\Lambda \ll B$), equations (3.4) and (3.5) reduce to those obtained by Mazouchi & Homsy (2000):

$$\tfrac{1}{3}H_{XXX}H^3 - \tfrac{1}{2}S(H^2 - B^2) = Ca_b(H - B) \quad \text{and} \quad Ca_b = SB^2. \tag{3.7a,b}$$

In (3.7*a*), taking $H \sim B$ and balancing the terms on the left-hand side, $B^4/X^3 \sim SB^2$ gives $B^2 \sim SX^3$. Also, because $X \sim B^{1/2}$ from $H(X \to \infty) \to X^2/2$ due to (3.6*b*), we arrive at $B \sim S^2$, which is (2.4). Equation (3.7*b*) then immediately gives $Ca_b \sim S^5$, which is (2.5). But a simple balance between the terms on both sides of (3.7*a*) will not give the correct scaling for Ca_b, which seems inconsistent. The reason is that, while the terms on the left-hand side are of the same order of magnitude SB^2, their difference is *not* SB^2 and actually goes an $O(B)$ higher like SB^3. This slight flow-rate mismatch balances the Ca_b term; so $SB^3 \sim Ca_bB$ gives the correct scaling $Ca_b \sim SB^2$ in accordance with (3.7*b*). Physically, the interface has to adjust its shape in such a way that the capillary flow $H^3H_{XXX}/3$ just slightly exceeds the thermocapillary flow $S(H^2 - B^2)/2$ to generate a little net flow to set the bubble in motion under the global conservation condition (3.7*b*).

In the strong-slip limit ($\Lambda \gg B$), (3.4) and (3.5) reduce to

$$\Lambda H^2 H_{XXX} - S\Lambda(H - B) = Ca_b(H - B) \quad \text{and} \quad Ca_b = 2\Lambda BS. \tag{3.8a,b}$$

Following similar arguments to those above, we find $B \sim S^2$ again and $Ca_b \sim \Lambda S^3$, and the latter is essentially (2.11). The crossover between the no-slip result $Ca_b \sim S^5$ and the strong-slip one $Ca_b \sim \Lambda S^3$ occurs at $S \sim \Lambda^{1/2}$, which is actually (2.9).

In terms of how to obtain the actual solution, we use (3.5) to replace Ca_b in terms of S and B in (3.4) and then solve (3.4) numerically with boundary conditions (3.6). Specifically, for a given S, we guess a value for B and then solve (3.4) subject to the initial conditions (3.6*a*) by shooting using the fourth-order Runge–Kutta method. We repeat the above procedures until the solution satisfies the far-distance condition (3.6*b*).

While the above solution procedures seem straightforward, we sometimes require a very accurate initial guess to obtain a correct solution behaviour, especially for S below 10^{-2}. The reason is that, for small S, not only is the film thickness H very small but also its slope H_X has to be very steep as it approaches the bubble cap in order to match the curvature of the cap via (3.6*b*): $H_{XX} \to 1$ as $X \to \infty$. Therefore, any small deviation of H might cause a significant overshooting or undershooting. From this point of view, we also seek a way to better lock on to the solution. To do so, noting that $H \sim S^2$ in both the no-slip and strong-slip limits, we rescale H and X in (3.4) as $\eta = H/S^2$ and $Z = X/S$ (because $X \sim H^{1/2}$ from (3.6*b*)), respectively, similar to previous studies on the same problem without slip (Wilson 1995; Mazouchi & Homsy 2000). Further, letting $\tilde{B} = B/S^2$ and $\tilde{\Lambda} = \Lambda/S^2$, (3.4) can be transformed into

$$\tfrac{1}{3}\eta_{ZZZ}(\eta^3 + 3\tilde{\Lambda}\eta^2) - \tfrac{1}{2}(\eta - \tilde{B})(\eta + \tilde{B} + 2\tilde{\Lambda}) = C(\eta - \tilde{B}), \tag{3.9}$$

with $C \equiv Ca_b/S^3 = S^2(\tilde{B}^2 + 2\tilde{\Lambda}\tilde{B})$. The boundary conditions (3.6) in the rescaled form remain unchanged. So in solving (3.4), H is small but X is kept $O(1)$. To have the solution behaviour correctly matched to (3.6*b*), B needs to be carefully adjusted with little errors allowed in the shooting. In contrast, in the rescaled form (3.9), we stretch both η and Z as $O(1)$. Since η_Z is now $O(1)$, the solution should be easily sought by simple shooting without any difficulty in matching $\eta_{ZZ} \to 1$ as $Z \to \infty$. In other words,

Downloaded from https://www.cambridge.org/core. National Cheng Kung University, on 21 Jul 2020 at 05:08:35, subject to the Cambridge Core terms of use, available at https://www.cambridge.org/core/terms. https://doi.org/10.1017/jfm.2014.117

because everything is kept $O(1)$, this allows us to ensure the solution behaviour by preventing possible inaccuracy from overshooting or undershooting. We have verified that it is indeed much easier to get an accurate solution by solving (3.9). As they should be, the results by solving the rescaled (3.9) are identical to those by solving (3.4), which is also confirmed.

4. Results and discussion

Figure 4(*a*) plots the film thickness B against the driving stress S for various values of Λ. At $\Lambda = 0$, we find that B scales like S^2, recovering the no-slip result (2.4) found by Mazouchi & Homsy (2000). When wall slip exists, even with a fractional amount like $\Lambda = 0.001$, we can clearly see that B starts to become lower than the no-slip case at $S \sim 10^{-2}$, which is about the critical stress $S^* \sim \Lambda^{1/2}$ (see (2.9)) below which B is smaller than Λ and slip effects become important. With further lowering of S, this decrease in B becomes even more pronounced. Yet, when S reaches 10^{-3} or smaller, the decrease becomes saturated, making B again approach like S^2 but with its value approximately $1/3$ smaller than in the no-slip case. For larger values of Λ, the results basically follow the above trend, but the transitions take place at larger values of S.

Figure 4(*a*) basically reveals that, even though B with wall slip is smaller than that without, its value in the very small S regime still scales like S^2, which confirms our scaling $B \sim S^2$ (2.4) in both the no-slip and strong-slip limits. For this reason, to make the transition from no slip to strong slip look more apparent, we plot B/S^2 against S in figure 4(*b*). It clearly shows that the curves basically vary in between the two horizontal asymptotes associated with the no-slip and strong-slip limits. Taking a closer look at the curves of $\Lambda = 0.0001$, 0.001 and 0.01, they have inflection points at $S \approx 2 \times 10^{-3}$, 10^{-2} and 2×10^{-2}, marking the corresponding crossover points between no-slip and strong-slip results. Taking the inflection points for various values of Λ in the range 10^{-4}–10^{-2} and plotting the corresponding S values against Λ in figure 5, we find that these values exactly scale like $\Lambda^{1/2}$, which confirms the crossover scaling (2.9).

Having obtained B as a function of S, we can readily determine Ca_b for finding the bubble speed using (3.5). The results with various values of Λ are displayed by plotting Ca_b against S in figure 6(*a*). At $\Lambda = 0$, we see that Ca_b scales like S^5, in accordance with the no-slip result (2.5) found by Mazouchi & Homsy (2000). At $\Lambda \neq 0$, we find that Ca_b can be increased by wall slip in such a way that $Ca_b \propto S^5$ can turn to $Ca_b \propto S^3$ when deceasing S from large to small values, clearly demonstrating a transition from the no-slip state to the strong-slip state. What is more striking is that, even with 1 % of wall slip ($\Lambda = 0.01$), the bubble speed for $S < 10^{-3}$ can be more than two orders of magnitude faster than without slip. It is also evident that the larger Λ, the faster the bubble moves. Plotting Ca_b/Λ against S in figure 6(*b*) collapses all the data in the small S regime perfectly, confirming the strong-slip scaling $Ca_b \sim \Lambda S^3$ predicted by (2.11).

5. Extension to polygonal tubes and connection to experiments

While the present work is based on the cylindrical tube geometry, we also seek an extension to other geometries as well as a connection to experiments. It is not difficult to anticipate that, for the present Bretherton-type problem, our findings can be equally applied to two-dimensional channels, except with different coefficients. But for other geometries such as polygonal tubes, Mazouchi & Homsy (2001) showed in their no-slip theory that the bubble speed can behave in a quite different way compared to

Downloaded from https://www.cambridge.org/core. National Cheng Kung University, on 21 Jul 2020 at 05:08:35, subject to the Cambridge Core terms of use, available at https://www.cambridge.org/core/terms. https://doi.org/10.1017/jfm.2014.117

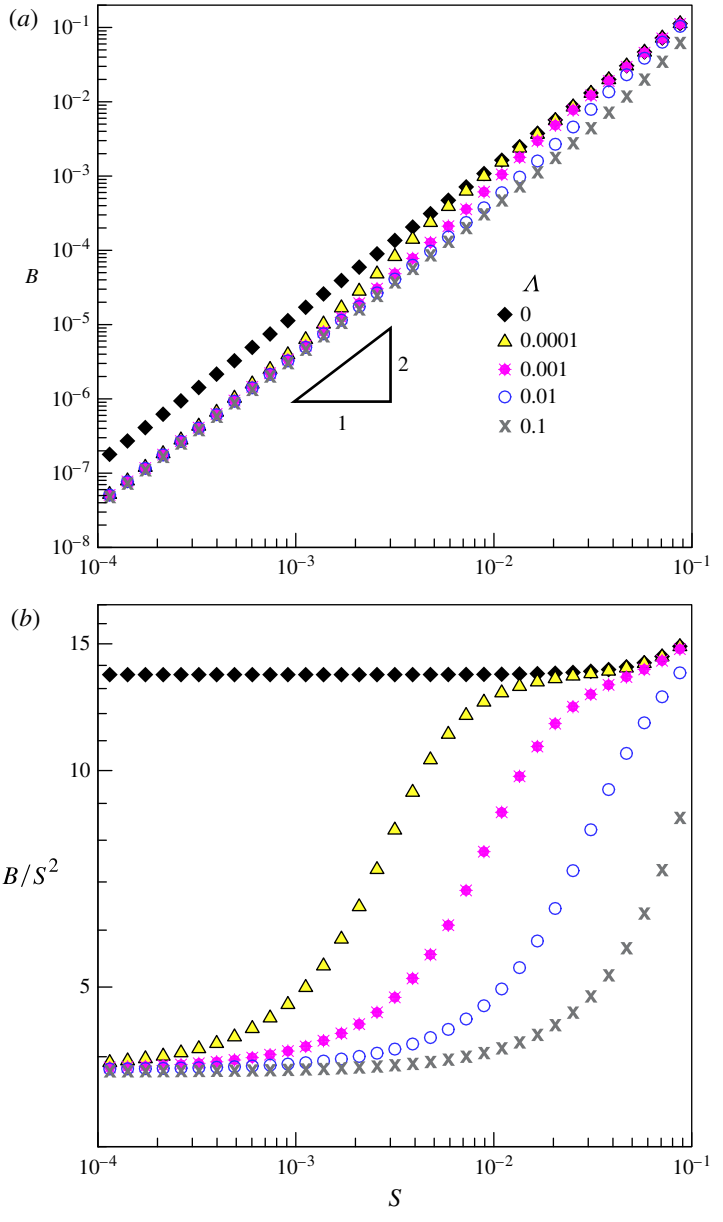

FIGURE 4. (*a*) Calculated film thickness $B = b/R$ as a function of $S = \tau_T R/\sigma_0$ for various values of the slip length $\Lambda = \lambda/R$. At $\Lambda = 0$, B is found to scale as S^2. At a given value $\Lambda \neq 0$, the curve starts to deviate from the no-slip one at some S on decreasing S from large to small values. In the very small-S regime like $S < 10^{-3}$, although wall slip effects are strong, all the curves show $B \sim S^2$ but with magnitude slightly smaller than the no-slip case. (*b*) The result of plotting B/S^2 against S, clearly showing that $B \sim S^2$ in both no-slip and strong-slip limits. Note that inflection points seem to exist at $S \approx 2 \times 10^{-3}$, 10^{-2} and 2×10^{-2} for the curves of $\Lambda = 0.0001$, 0.001 and 0.01, marking transitions from the no-slip state to the strong-slip state.

Downloaded from https://www.cambridge.org/core. National Cheng Kung University, on 21 Jul 2020 at 05:08:35, subject to the Cambridge Core terms of use, available at https://www.cambridge.org/core/terms.
https://doi.org/10.1017/jfm.2014.117

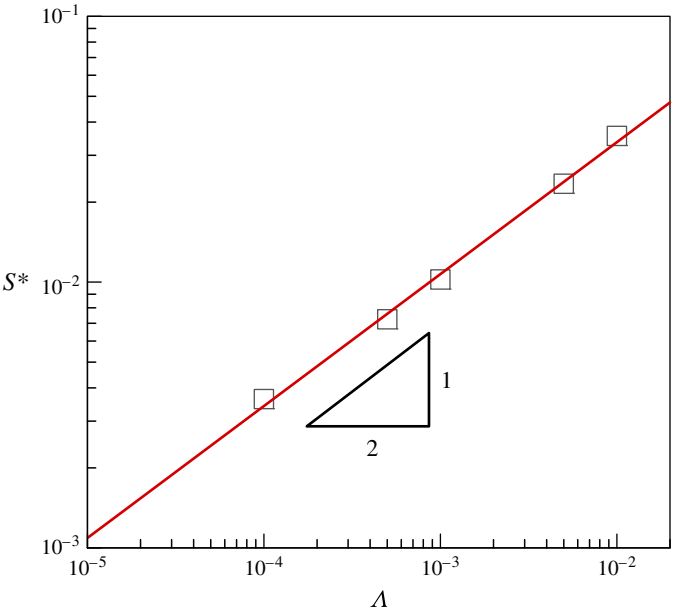

FIGURE 5. Plot of S^*, the transition point from the no-slip state to the strong-slip state, against Λ, showing $S^* \sim \Lambda^{1/2}$ in agreement with (2.9). Here the values of S^* are taken from the inflection points seen in figure 4(*b*) for $\Lambda = 10^{-4}$–10^{-2}.

that in a circular tube. They found that, instead of (2.5), the bubble speed, in our notation, takes the form

$$\frac{\mu}{\sigma_0} U_b = c_1 \frac{a\tau_T}{\sigma_0} + c_2 \left(\frac{a\tau_T}{\sigma_0}\right)^5, \tag{5.1}$$

where $a\tau_T/\sigma_0$ is roughly like our S, with a being the characteristic dimension (e.g. the radius of the mean curvature of the bubble surface around a corner sector), and c_1 and c_2 are dimensionless coefficients that depend on the shape of the tube cross-section. They identified that the bubble speed mainly comes from the $O(a\tau_T/\sigma_0)$ term due to the thermocapillary flow through the corner regions of the tube, plus the $O((a\tau_T/\sigma_0)^5)$ correction due to the neighbouring thin films. Note that the $O((a\tau_T/\sigma_0)^5)$ correction is exactly (2.5). In the subsequent experimental study using rectangular channels, Lajeunesse & Homsy (2003) found that the measured bubble speed roughly grows linearly with the applied temperature gradient, as described by the first term of (5.1). So the geometry of the tube cross-section seems to play an important role in the movement of the bubble.

When wall slip is present, we expect that more terms should be added to (5.1) to account for slip effects. Here we do not intend to solve this problem. Instead, we make some rational guesses about how (5.1) is modified. As explained in the Appendix, we postulate the following expression for the bubble speed in a slippery polygonal tube:

$$\frac{\mu}{\sigma_0} U_b = c_1 \frac{a\tau_T}{\sigma_0} \left(1 + d_1 \left(\frac{\lambda}{w}\right)\right) + c_2 \left(\frac{a\tau_T}{\sigma_0}\right)^5 \left(1 + d_2 \left(\frac{\lambda}{a}\right) \left(\frac{a\tau_T}{\sigma_0}\right)^{-2}\right). \tag{5.2}$$

Downloaded from https://www.cambridge.org/core. National Cheng Kung University, on 21 Jul 2020 at 05:08:35, subject to the Cambridge Core terms of use, available at https://www.cambridge.org/core/terms.
https://doi.org/10.1017/jfm.2014.117

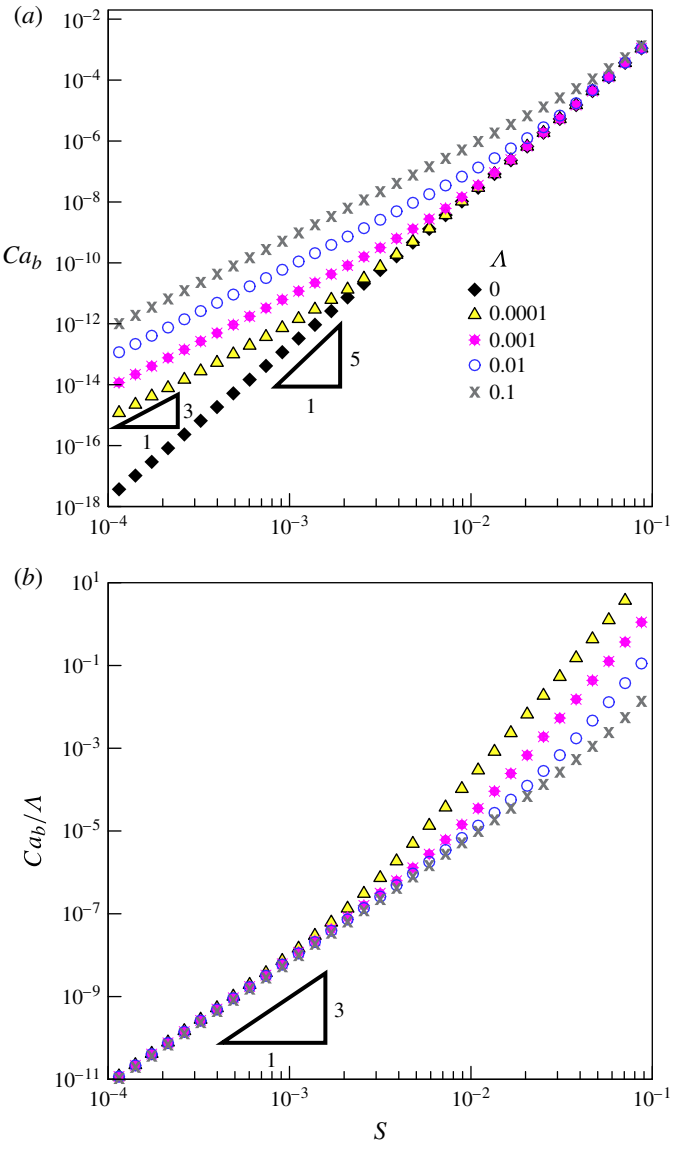

FIGURE 6. (*a*) Calculated bubble capillary number Ca_b against S for various values of Λ. Here Ca_b is evaluated using (3.5) using the calculated values of B shown in figure 4. The no-slip case $\Lambda = 0$ shows $Ca_b \sim S^5$. At $\Lambda \neq 0$, Ca_b can be increased by wall slip in such a way that $Ca_b \propto S^5$ can turn to $Ca_b \propto S^3$ when decreasing S from large to small values, clearly demonstrating a transition from the no-slip state to the strong-slip state. (*b*) The data in the small-S regime can be collapsed by plotting Ca_b/Λ against S, confirming $Ca_b \sim \Lambda S^3$ shown by (2.11).

Here two additional slip terms, λ/w and $(\lambda/a)(a\tau_T/\sigma_0)^{-2}$ (with $O(1)$ coefficients d_1 and d_2), are added to the c_1 and c_2 terms, respectively, where w ($< a$) is the gap size between the bubble surface and the wall in the corner region. Note that the actual c_1 value can be hundreds or thousands of times *smaller* than c_2, depending on the tube geometry (Mazouchi & Homsy 2001). Since $a\tau_T/\sigma_0$ is typically small, the inclusion

Downloaded from https://www.cambridge.org/core. National Cheng Kung University, on 21 Jul 2020 at 05:08:35, subject to the Cambridge Core terms of use, available at https://www.cambridge.org/core/terms.
https://doi.org/10.1017/jfm.2014.117

of the slip terms might change the relative importance between the c_1 and c_2 terms when slip effects are important.

In terms of experiments, we take the conditions in the study of Lajeunesse & Homsy (2003) to estimate the parameters involved and to identify how wall slip changes the relative importance between the terms in (5.2). In their study, the tube size is $a \sim 1$ mm. The fluid viscosity is $\mu \approx 10^{-4}$–10^{-3} Pa s. The surface tension is $\sigma_0 \approx 10^{-2}$ N m^{-1} with the temperature coefficient $\beta \approx 10^{-5}$ N m^{-1} K^{-1}. The temperature gradient across the bubble is $G_b \approx 10^2$ K m^{-1}. Using the above data, we have $\tau_T a/\sigma_0 = \beta G_b a/\sigma_0 \approx 10^{-4}$. For the channels that they used, $c_1 \approx 10^{-2}$–10^{-3} and $c_2 \approx 1$–10. As also shown in the Appendix, we find that the bubble speed, with and without wall slip, is always dominated by the c_1 term. In the absence of wall slip, the bubble speed can be estimated using the c_1 term of (5.1), giving $U_b \approx 1$–100 μm s^{-1}. If wall slip exists especially when a polymeric liquid is used (de Gennes 1985), the slip length can be as large as $\lambda \sim 1$ μm (which is much larger than the film thickness b estimated by $b \sim a(\tau_T a/\sigma_0)^2$ according to (2.4)). If the liquid thickness in the corner sectors w happened to be comparable to or smaller than λ, it is possible to increase the bubble speed according to the c_2 term of (5.2).

It is worth pointing out that in the above discussion, we assume that τ_T is a constant by taking the temperature gradient across the bubble G_b to be roughly the global temperature gradient G so that the bubble speed can always be described by (5.2). However, if we use this way and apply $b \approx 10a(\beta G_b a/\sigma_0)^2$ obtained by Mazouchi & Homsy (2001) to estimate the film thickness in the experiments of Lajeunesse & Homsy (2003), we find that b is of the order of angstroms, which is actually unphysically too thin compared to the film thickness (whose thinnest part is estimated to be of the order of micrometres) seen in their experiments. Perhaps a way to resolve this is to assume that the bubble is nearly insulated and its length is much shorter than the channel length, so that a much thicker film can be rendered by the much greater driving stress $\tau_T \sim G_b\beta \sim (a/b)G\beta$ due to the much intensified temperature gradient over the bubble surface $G_b \sim (a/b)G$ (see § 2.1). By doing so, the film thickness will scale like Bretherton's law, $b \sim a(\beta G a/\sigma_0)^{2/3}$ (see (2.7)), giving b of the order of micrometres under $G \approx 10^2$ K m^{-1}. Using $a\tau_T/\sigma_0 = \beta G_b a/\sigma_0 \sim (\beta G a/\sigma_0)^{1/3}$ based on Bretherton's law, (5.2) is transformed into

$$\frac{\mu}{\sigma_0}U_b = c_1\left(\frac{G\beta a}{\sigma_0}\right)^{1/3}\left(1 + d_1\left(\frac{\lambda}{w}\right)\right) + c_2\left(\frac{G\beta a}{\sigma_0}\right)^{5/3}\left(1 + d_2\left(\frac{\lambda}{a}\right)\left(\frac{G\beta a}{\sigma_0}\right)^{-2/3}\right), \tag{5.3}$$

which makes the dependence of U_b on G less strong. In the c_2 term, the slip term can become important when

$$\beta G a/\sigma_0 < (\lambda/a)^{3/2}. \tag{5.4}$$

In this case, even if the c_1 term is dominated by the no-slip term, the c_2 term can still win because its ratio to the c_1 term, $(c_2/c_1)(\lambda/a)(\beta G a/\sigma_0)^{2/3} \sim 10(\lambda/a)$, can become greater than unity with $c_2/c_1 = 10^4$ (using channels with large aspect ratios or circular tubes) and $\beta G a/\sigma_0 \sim 10^{-4}$. The resulting bubble speed is then governed by

$$\frac{\mu}{\sigma_0}U_b \approx c_2 d_2\left(\frac{G\beta a}{\sigma_0}\right)\left(\frac{\lambda}{a}\right), \tag{5.5}$$

which is essentially (2.13). More importantly, the bubble speed still varies *linearly* with the applied temperature gradient. Perhaps for this reason, the bubble speeds measured in the study by Lajeunesse & Homsy (2003) can sometimes display slightly higher values than those predicted by the no-slip model (see their figure 6).

Downloaded from https://www.cambridge.org/core. National Cheng Kung University, on 21 Jul 2020 at 05:08:35, subject to the Cambridge Core terms of use, available at https://www.cambridge.org/core/terms.
https://doi.org/10.1017/jfm.2014.117

6. Concluding remarks

We have demonstrated that wall slip can have a profound impact on the thermocapillary motion of a long bubble in a closely fitting tube. We find that, although the film thickness does not change much with the extent of wall slip, the bubble can be significantly speeded up by slip effects. As shown in figure 6(*a*), at sufficiently low driving thermal stress $S = \tau_T R/\sigma_0$ like 10^{-3} or smaller, a mere 1 % of wall slip ($\Lambda \equiv \lambda/R = 0.01$) can make the bubble travel more than 100 times faster than in the no-slip case. This is attributed to the fact that the bubble speed $U_b \sim (\sigma_0/\mu)\Lambda S^3$ in the strong-slip state is ΛS^{-2} greater than the $U_b \sim (\sigma_0/\mu)S^5$ in the no-slip state. Therefore, with the help of wall slip, bubbles can quite easily be driven by small temperature gradients. In other words, to reach the same bubble speed, the required temperature with slip will be considerably smaller than that without slip gradient. For instance, to have the bubble speed at a level like $Ca_b = 10^{-10}$, the driving stress $S \approx 10^{-3}$ at $\Lambda = 0.01$ is approximately four times smaller than that at $\Lambda = 0$. If the bubble length is much shorter than the tube length, the actual temperature gradient across the bubble will be amplified by a factor R/b. In this case, written in terms of the global temperature gradient G, since $G \propto S^3$ due to $S = \frac{1}{2}(G\beta R/\sigma_0)/B$ (see the remark after (3.4)) and $B \sim S^2$, the required global temperature difference can be reduced by more than 100 times!

Moreover, we find that there exists a *super*-slip regime (see § 2.3) where the bubble can also be speeded up by slip effects in a different manner but cannot be captured by the standard lubrication analysis. Specifically, this happens in the situation where the film is ultrathin such that its lateral size ℓ becomes much smaller than the slip length λ. In this case, the bubble speed is found to scale as (2.17). It is somewhat surprising that (2.17) is actually *slower* than the strong-slip case (2.13) (while it is still faster than the no-slip case (2.8)). The reason is that the bubble motion here is dissipated viscously not over the film thickness but over the much longer lateral side of the film. For much larger slip length like $\lambda \gg R$, the wall of the tube has no influence on the bubble, thereby making the bubble migrate as if it were in an unbounded fluid.

While our analysis is based on a circular tube geometry, it should also be applicable to slit-like channels (Mazouchi & Homsy 2001). So our findings also hold for this geometry. For other geometries, we extend our analysis to polygonal tubes by adding slip terms to the expression for the bubble speed derived by Mazouchi & Homsy (2001) (see § 5). We find that, as long as the bubble is nearly insulated and its length is much shorter than the length of the tube, it is possible to increase the bubble speed by slip effects in the manner similar to what Mazouchi & Homsy (2001) observed in their experiments. As the flow is basically controlled by the film, we also expect that our results should also be applicable to a liquid droplet provided that its thermal conductivity is much lower than that of the continuous phase. On the other hand, if one would like to conduct an experiment to see whether the drop speed U can change its dependence on the applied temperature gradient G due to wall slip, perhaps it can be achieved by: (i) the use of a cylindrical tube or a shallow microchannel having a large width-to-depth ratio for eliminating corner sector effects, and (ii) choosing the drop phase to be thermally conductive so that the temperature gradient across the drop can be made comparable to that across the length of a tube/microchannel.

In terms of microfluidic applications, it might also be desirable to utilise slip effects to enhance fluidic transport (such as pumping and mixing) in thermally actuated devices. As apparent wall slip can be generated much more easily by surface functionalisation or textures, our results might provide useful guidance for designing such devices.

Downloaded from https://www.cambridge.org/core. National Cheng Kung University, on 21 Jul 2020 at 05:08:35, subject to the Cambridge Core terms of use, available at https://www.cambridge.org/core/terms. https://doi.org/10.1017/jfm.2014.117

In a broader perspective, we have previously demonstrated that wall slip can drastically modify flow characteristics and give rise to no-slip to slip transitions for a number of free-surface flows (Liao *et al.* 2013). We show that the same things can also happen to stress-driven flows as considered here. In particular, we find that our findings for the present thermocapillary problem are equivalent to those of the Bretherton problem (Liao *et al.* 2013) (see § 2.4), meaning that, though driven by different mechanisms, the essential physics of these two problems are basically the same. As the features of such Bretherton-type problems can also be used to describe other processes such as dip coating and drop spreading (Stone 2010; Liao *et al.* 2013), we believe that the impact of wall slip could be quite universal to a wide class of interfacial flows – all are sensitive to the amount of wall slip. As the transition from no-slip to strong slip always occurs when the film thickness is comparable to the slip length ($b \sim \lambda$), the associated scaling at the transition point would provide not only a criterion to evaluate the importance of slip effects, but also a direct link between the microscopic slip length and the macroscopic length scales. Also because such a crossover scaling is unique for a given flow system, it might offer a more reliable means to quantify the amount of slip experimentally. As slip effects would manifest most when $b < \lambda$, molecular effects (e.g. disjoining pressure) between the bubble surface and the tube wall might come into play to mediate flow characteristics at the scale of 100 nm or smaller (de Gennes, Brochard-Wyart & Quéré 2003). So it would be interesting to see how such effects influence the bubble speed found in the present work, which will be pursued in our future study.

Acknowledgement

This work is supported by the National Science Council of Taiwan under grant no. 101-2221-E-006-230-MY3 to H.H.W.

Appendix. Effects of wall slip on the thermocapillary speed of a long bubble in a polygonal tube

This appendix is to provide plausible conjectures about how wall slip effects modify the no-slip result (5.1) found by Mazouchi & Homsy (2001). Because of the slip length λ, there must be additional terms involving λ/a (like our Λ) in (5.1). First consider the c_1 term in (5.1). This term accounts for the thermocapillary flow through the corner sectors enclosed by the tube walls and the bubble surface. Since the bubble surface in these regions is always kept hydrostatic (in the small-capillary-number regime) (Mazouchi & Homsy 2001), its shape will not change at all. In other words, the total cross-sectional area in such regions remains unchanged. So the associated flow rate can be increased by a factor of $O(\lambda/a)$ due to wall slip. As for the c_2 term from the thin-film correction, wall slip can make the film thinner. But such film thinning should not be too sensitive to the shape of the tube cross-section (which has already been reflected by c_2). So we expect that this term should be modified into the form like (3.5) with $B \sim S^2$. Combining the above reasonings, we modify (5.1) by adding the respective slip terms to both the c_1 and c_2 terms as

$$\frac{\mu}{\sigma_0} U_b = c_1 \frac{a\tau_T}{\sigma_0} \left(1 + d_1' \left(\frac{\lambda}{a}\right)\right) + c_2 \left(\frac{a\tau_T}{\sigma_0}\right)^5 \left(1 + d_2 \left(\frac{\lambda}{a}\right) \left(\frac{a\tau_T}{\sigma_0}\right)^{-2}\right). \quad \text{(A 1)}$$

But a closer inspection of the slip term in the c_1 term reveals that the actual magnitude of this term is not necessarily $O(\lambda/a)$ because the coefficient d_1' could

Downloaded from https://www.cambridge.org/core. National Cheng Kung University, on 21 Jul 2020 at 05:08:35, subject to the Cambridge Core terms of use, available at https://www.cambridge.org/core/terms. https://doi.org/10.1017/jfm.2014.117

be large, depending on the gap size between the wall and the bubble surface of a corner sector, w. Because w is no more than $O(a)$, we can consider two situations: (i) $w \sim O(a)$ and (ii) $w \ll O(a)$. In (i), $d_1' \sim O(1)$, so the slip term is merely a correction. But in (ii), the fluid now is confined by a much smaller gap, so it may see more influence from the slippery wall when $w < \lambda$. In this case, the flow is speeded up by a much larger factor λ/w, giving $d_1' \sim O(a/w)$. So in any case we can always set $d_1' = (a/w)d_1$ with $d_1 = O(1)$ for the c_1 term. Hence, the c_1 term can be rewritten as

$$c_1 \left(\frac{a\tau_T}{\sigma_0}\right)\left(1 + d_1\left(\frac{\lambda}{w}\right)\right). \tag{A 2}$$

Combining (A 1) and (A 2) thus yields (5.2).

As the inclusion of the slip terms might change the relative importance between the c_1 and c_2 terms, we use the ratio Ω of the c_2 term to the c_1 term to see which term dominates in (A 1).

In the no-slip limit, $\Omega(\lambda = 0) \sim (c_2/c_1)(a\tau_T/\sigma_0)^4$. So even though c_2/c_1 can be as large as 10^4, $a\tau_T/\sigma_0$ is typically 10^{-4} or smaller (Lajeunesse & Homsy 2003). This leads to $\Omega(\lambda = 0) \sim 10^{-12}$ and hence the bubble speed is dominated by the c_1 term. This explains why U_b is roughly linear in τ_T in the study of Lajeunesse & Homsy (2003).

When wall slip is present, even with a fraction of wall slip like $\lambda/a \sim 10^{-2}$, one can have $a\tau_T/\sigma_0 < (\lambda/a)^{1/2}$ to make the c_2 term dominated by the slip term $(\lambda/a)(a\tau_T/\sigma_0)^3$. In this case, because the c_1 term is also increased due to the λ/w term, $\Omega(\lambda \neq 0)$ ranges between $\Omega \sim (c_2/c_1)(\lambda/a)(a\tau_T/\sigma_0)^2$ for $w > \lambda$ and $\Omega \sim (c_2/c_1)(w/a)(a\tau_T/\sigma_0)^2$ for $w < \lambda$. Even if the largest values $c_2/c_1 \sim 10^4$ and $a\tau_T/\sigma_0 \sim 10^{-4}$ are used (Lajeunesse & Homsy 2003), $\Omega(\lambda \neq 0)$ is still much smaller than unity. So we conclude that the bubble speed, with and without wall slip, is always dominated by the c_1 term.

Note that the dominance of the c_1 term in (A 1) shown above is based on the assumption that τ_T is a constant by taking the temperature gradient across the bubble G_b to be roughly the global temperature gradient G. However, this assumption will no longer hold if the bubble is moving in a much longer channel in which G_b is amplified like $G_b \sim (a/b)G$ to give $\tau_T \sim (a/b)G\beta$ (see (2.6)). In this case, the bubble speed can be dominated by the slip part of the c_2 term, as seen in the discussion at the end of § 5.

REFERENCES

Baroud, C. N., Delville, J.-P., Gallaire, F. & Wunenburger, R. 2007 Thermocapillary valve for droplet production and sorting. *Phys. Rev.* E **75**, 046302.

Bretherton, F. P. 1961 The motion of long bubbles in tubes. *J. Fluid Mech.* **10**, 166–188.

Brochard-Wyart, F., Debrégeas, G. & de Gennes, P. G. 1996 Spreading of viscous droplets on a non-viscous liquid. *Colloid Polym. Sci.* **274**, 70–72.

Brzoska, J. B., Brochard-Wyart, F. & Rondelez, F. 1993 Motions of droplets on hydrophobic model surfaces induced by thermal gradients. *Langmuir* **9**, 2220–2224.

Choi, C.-H. & Kim, C.-J. 2006 Large slip of aqueous liquid flow over a nanoengineered superhydrophobic surface. *Phys. Rev. Lett.* **96**, 066001.

Craig, V. S. J., Neto, C. & Williams, D. R. M. 2001 Shear-dependent boundary slip in an aqueous Newtonian liquid. *Phys. Rev. Lett.* **87**, 054504.

Downloaded from https://www.cambridge.org/core. National Cheng Kung University, on 21 Jul 2020 at 05:08:35, subject to the Cambridge Core terms of use, available at https://www.cambridge.org/core/terms. https://doi.org/10.1017/jfm.2014.117

DARHUBER, A. A., VALENTINO, J. P., TROIAN, S. M. & WAGNER, S. 2003 Thermocapillary actuation of droplets on chemically patterned surfaces by programmable microheater arrays. *J. Microelectromech. Syst.* **12**, 873–879.

DE GENNES, P. G. 1985 Wetting: statics and dynamics. *Rev. Mod. Phys.* **57**, 827–863.

DE GENNES, P. G., BROCHARD-WYART, F. & QUÉRÉ, D. 2003 *Capillarity and Wetting Phenomena: Drops, Bubbles, Pearls, Waves*. Springer.

GOMBA, J. M. & HOMSY, G. M. 2010 Regimes of thermocapillary migration of droplets under partial wetting conditions. *J. Fluid Mech.* **647**, 125–142.

HOMSY, G. M. 1987 Viscous fingering in porous media. *Annu. Rev. Fluid Mech.* **19**, 271–311.

HU, G.-H. 2005 Linear stability of ultrathin slipping films with insoluble surfactant. *Phys. Fluids* **17**, 088105.

JIAO, Z., HUANG, X., NGUYEN, N.-T. & ABGRALL, P. 2008 Thermocapillary actuation of a droplet in a planar microchannel. *Microfluid. Nanofluid.* **5**, 205–214.

KARAPETSAS, G., SAHU, K. C. & MATAR, O. K. 2013 Effect of contact line dynamics on the thermocapillary motion of a droplet on an inclined plate. *Langmuir* **29**, 8892–8906.

KARGUPTA, K., SHARMA, A. & KHANNA, R. 2004 Instability, dynamics and morphology of thin slipping film. *Langmuir* **20**, 244–253.

LAJEUNESSE, E. & HOMSY, G. M. 2003 Thermocapillary migration of long bubbles in polygonal tubes. II. Experiments. *Phys. Fluids* **15**, 308–314.

LAUGA, E., BRENNER, M. P. & STONE, H. A. 2007 Microfluidics: the no-slip boundary condition. In *Springer Handbook of Experimental Fluid Mechanics* pp. 1219–1240. Springer.

LI, Y.-C., LIAO, Y.-C., WEN, T.-C. & WEI, H.-H. 2014 Breakdown of the Bretherton law due to wall slippage. *J. Fluid Mech.* **741**, 200–227.

LIAO, Y.-C., LI, Y.-C. & WEI, H.-H. 2013 Drastic changes in interfacial hydrodynamics due to wall slippage: slip-intensified film thinning, drop spreading, and capillary instability. *Phys. Rev. Lett.* **111**, 136001.

MAZOUCHI, A. & HOMSY, G. M. 2000 Thermocapillary migration of long bubbles in cylindrical capillary tubes. *Phys. Fluids* **12**, 542–549.

MAZOUCHI, A. & HOMSY, G. M. 2001 Thermocapillary migration of long bubbles in polygonal tubes. I. Theory. *Phys. Fluids* **13**, 1594–1600.

MÜNCH, A. 2005 Dewetting rates of thin liquid films. *J. Phys.: Condens. Matter* **17**, S309–S318.

MÜNCH, A. & WAGNER, B. 2005 Contact-line instability of dewetting thin films. *Physica* D **209**, 178–190.

MÜNCH, A., WAGNER, B. & WITELSKI, T. P. 2005 Lubrication models with small to large slip lengths. *J. Engng Math.* **53**, 359–383.

NAVIER, C. L. M. H. 1823 Mémoire sur les lois du mouvement des fluids. *Mém. Présentés par Divers Savants Acad. Sci. Inst. Fr.* **6**, 389–440.

NGUYEN, H.-B. & CHEN, J.-C. 2010 A numerical study of thermocapillary migration of a small liquid droplet on a horizontal solid surface. *Phys. Fluids* **22**, 062102.

PRATAP, V., MOUMEN, N. & SUBRAMANIAN, R. S. 2008 Thermocapillary motion of a liquid drop on a horizontal solid surface. *Langmuir* **24**, 5185–5193.

SAFFMAN, P. G. & TAYLOR, G. 1958 The penetration of a fluid into a porous medium or Hele-Shaw cell containing a more viscous liquid. *Proc. R. Soc. Lond.* A **245**, 312–329.

SELVA, B., MIRALLES, V., CANTAT, I. & JULLIEN, M.-C. 2010 Thermocapillary actuation by optimised resistor pattern: bubbles and droplets, displacing, switching and trapping. *Lab on a Chip* **10**, 1835–1840.

SHARMA, A. & KARGUPTA, K. 2003 Instability and dynamics of thin slipping films. *Appl. Phys. Lett.* **83**, 3549–3551.

SLATTERY, J. C. 1974 Interfacial effects in the entrapment and displacement of residual oil. *AIChE J.* **20**, 1145–1154.

SMITH, M. K. 1995 Thermocapillary migration of a two-dimensional liquid droplet on a solid surface. *J. Fluid Mech.* **294**, 209–230.

STONE, H. A. 2010 Interfaces: in fluid mechanics and across disciplines. *J. Fluid Mech.* **645**, 1–25.

Downloaded from https://www.cambridge.org/core. National Cheng Kung University, on 21 Jul 2020 at 05:08:35, subject to the Cambridge Core terms of use, available at https://www.cambridge.org/core/terms. https://doi.org/10.1017/jfm.2014.117

SUBRAMANIAN, R. S. 1981 Slow migration of a gas bubble in a thermal gradient. *AIChE J.* **27**, 646–654.

TYRRELL, J. W. G. & ATTARD, P. 2001 Images of nanobubbles on hydrophobic surfaces and their interactions. *Phys. Rev. Lett.* **87**, 176104.

WILSON, S. K. 1993 The steady thermocapillary-driven motion of a large droplet in a closed tube. *Phys. Fluids* A **5**, 2064–2066.

WILSON, S. K. 1995 The effect of an axial temperature gradient on the steady motion of a large droplet in a tube. *J. Engng Math.* **29**, 205–217.

YOUNG, N. O., GOLDSTEIN, J. S. & BLOCK, M. J. 1959 The motion of bubbles in a vertical temperature gradient. *J. Fluid Mech.* **6**, 350–356.

Downloaded from https://www.cambridge.org/core. National Cheng Kung University, on 21 Jul 2020 at 05:08:35, subject to the Cambridge Core terms of use, available at https://www.cambridge.org/core/terms. https://doi.org/10.1017/jfm.2014.117